applied sciences

MDPI

Communication

Game Theory in Molecular Nanosensing System for Rapid Detection of Hg^{2+} in Aqueous Solutions

Nan Fang Nie †, Xin Xing Zhang †, Chu Shan Fang, Qiu Yan Zhu, Jiao Yang Lu, Fu Rui Zhang, Qing Feng Yao, Wei Tao Huang *, Xue Zhi Ding and Li Qiu Xia

State Key Laboratory of Developmental Biology of Freshwater Fish, Hunan Provincial Key Laboratory of Microbial Molecular Biology, College of Life Science, Hunan Normal University, Changsha 410081, China; N2944626564@163.com (N.F.N.); zxx02215@163.com (X.X.Z.); F745317040@163.com (C.S.F.); 18199765199@163.com (Q.Y.Z.); joyceway@163.com (J.Y.L.); furui912443212@163.com (F.R.Z.); 17136373635@163.com (Q.F.Y.); dingxuezhi@hunnu.edu.cn (X.Z.D.); xialq@hunnu.edu.cn (L.Q.X.)

* Correspondence: vthuang@hunnu.edu.cn; Tel.: +86-731-8887-2905

† These authors contributed equally to this work and should be considered co-first authors.

Received: 5 November 2018; Accepted: 6 December 2018; Published: 7 December 2018

Abstract: Game theory—the scientific study of interactive, rational decision making—describes the interaction of two or more players from macroscopic organisms to microscopic cellular and subcellular levels. Life based on molecules is the highest and most complex expression of molecular interactions. However, using simple molecules to expand game theory for molecular decision-making remains challenging. Herein, we demonstrate a proof-of-concept molecular game-theoretical system (molecular prisoner's dilemma) that relies on formation of the thymine–Hg^{2+}–thymine hairpin structure specifically induced by Hg^{2+} and fluorescence quenching and molecular adsorption capacities of cobalt oxyhydroxide (CoOOH) nanosheets, resulting in fluorescence intensity and distribution change of polythymine oligonucleotide 33-repeat thymines (T33). The "bait" molecule, T33, interacted with two molecular players, CoOOH and Hg^{2+}, in different states (absence = silence and presence = betrayal), regarded as strategies. We created conflicts (sharing or self-interest) of fluorescence distribution of T33, quantifiable in a 2×2 payoff matrix. In addition, the molecular game-theoretical-system based on T33 and CoOOH was used for sensing Hg^{2+} over the range of 20 to 600 nM with the detection limit of 7.94 nM (3σ) and for determination of Hg^{2+} in pond water. Inspired by the proof-of-concept for molecular game theory, various molecular decision-making systems could be developed, which would help promote molecular information processing and generating novel molecular intelligent decision systems for environmental monitoring and molecular diagnosis and therapy.

Keywords: cobalt oxyhydroxide nanosheets; fluorescent sensing; game theory; Hg^{2+}; thymine–Hg^{2+}–thymine

1. Introduction

Game theory—the mathematical modeling of the strategic interaction between rational decision-makers—describes the interaction of two or more agents (or players), where the payoff for each player is determined not only by their own decision, but also by the strategies adopted by the coplayers [1]. There are various game types, including the prisoner's dilemma, hawk-dove game, battle of the sexes, and harmony games. Game theory originated in economics, but is today an interdisciplinary area of study, including political science, psychology, logic, and even biology [2]. For example, evolutionary game theory, which is derived from the combination of game theory and biology, has been under development for decades to focus on the interactions among macroscopic organisms [3]. Not only macroscopic organisms as a whole but also cells [1] and some macromolecules (RNAs [4], viruses [5], proteins) [6] within cells can be considered as players in game theory [6].

Life based on molecules is the highest and most complex expression of molecular interaction [7]. However, the molecular (or chemical) level has not been as well explored in game theory as interactions among macroscopic organisms or cells. As stated by Richard Feynman, for various interdisciplinary sciences, there is also plenty of room at the bottom [8]. Inspired by the natural logic of various information flows in life [9], simple biological systems and artificial molecular systems have been abstracted to develop biological [10,11] or molecular computing devices, such as Boolean logic circuits [12,13], neural network computation [14,15], and molecular security systems [16–19], by utilizing engineered biological units (such as the living cell) as building blocks in life systems [10,11], biochemical molecules nucleic acids [14,15,20], or organic molecules [16,18] in complex chemical systems. However, using simple molecules to expand game theory for molecular decision-making remains a challenge.

The interaction between simple molecules offers a unique opportunity to expand game theory, such as the prisoner's dilemma, because molecular interactions (molecular competition, synergy, or decomposition) between two or more molecular players will create conflicts ("silent" or "betray") similar to those assumed in game theory [21]. Cognitive and rational capabilities are not prerequisites of players in game-theoretical models [6]. Thus, molecules with different states (regarded as strategies or decisions) can generate different outcomes of the whole system and individuals, which are described using a payoff matrix. From the perspective of combinatorial chemistry, nucleic acids with compositional and conformational diversity have various molecular interaction capabilities, such as specific recognition of aptamers [22], catalytic activity of DNAzymes [23], and interaction of DNA bases with metal ions [24]. For example, thymine–Hg^{2+}–thymine (T–Hg^{2+}–T) and cytosine–Ag^{+}–cytosine (C–Ag^{+}–C), have drawn considerable attention in sensing [24] and logic computing applications [25]. Because Hg^{2+} is capable of selectively coordinating T bases and forms a strong and stable T–Hg^{2+}–T mismatch [26], there is increasingly interest [27,28] in the combination of T–Hg^{2+}–T [29] and nanomaterials (gold nanoparticles [30,31], graphene oxide [32], MoS_2 [33], and quantum dots [34]) for Hg^{2+} sensing [35]. The combination not only provides a more accurate strategy for molecular sensing (such as reversible dual-signal sensing [36]), but also provides a universal and convenient model and platform to study molecular game theory.

Herein, we demonstrate a successful example of the application of game theory (prisoner's dilemma) to interactions among simple molecules, which relies on the hairpin structure of polythymine oligonucleotide 33-repeat thymines (T33) specifically induced by Hg^{2+} and fluorescence quenching and molecular adsorption capacities of cobalt oxyhydroxide (CoOOH) nanosheets [37], resulting in fluorescence intensity and distribution change in T33. Two molecular players, CoOOH and Hg^{2}, with different states (absence = silence or presence = betrayal), regarded as strategies, interact with the "bait" molecule T33 and create conflicts (sharing or self-interest) of fluorescence distribution of T33, quantifiable in a 2 × 2 payoff matrix. Because both CoOOH and Hg^{2+} competitively interact with T33 to form a T–Hg^{2+}–T–CoOOH ternary complex, resulting in the largest signal change of the system, the molecular game-theoretical system was used to sensitively and selectively sense Hg^{2+}. Inspired by the proof-of-concept of the feasibility of molecular game theory, a variety of molecular decision-making devices can be developed and applied, creating a new field of interdisciplinary science that would help to break through the traditional information processing paradigm and aid in the development of novel molecular intelligent decision systems for environmental monitoring and molecular diagnosis and therapy.

2. Experiment Materials and Methods

2.1. Materials and Reagents

The oligonucleotides used in this study were synthesized by Sangon Biotechnology Co., Ltd. (Shanghai, China), they have a carboxyfluorescein (FAM)-label on the 5′ end, and the sequences were composed of 33-repeat thymines (T33). Cobaltous chloride ($CoCl_2 \cdot 6H_2O$) was obtained from

Sinopharm Chemical Reagent Co., Ltd. (Shanghai, China). Tris (hydroxymethyl) aminomethane (Tris), NaOH, NaClO, acridine orange, fluorescein, rhodamine B, eosin Y, calcein, and all of the metal salts used in this work were purchased from Aladdin Reagents Co., Ltd. (Shanghai, China). All reagents were of analytical grade. Hg^{2+} stock solution (10 mM) was prepared by dissolving $Hg(NO_3)_2$ with 0.5% HNO_3. All reagents were used as received without further purification. All aqueous solutions were prepared with ultrapure water, which was provided by a Millipore Milli-Q water purification system (Bedford, MA, USA) and had an electric resistance >18.2 MΩ·cm.

2.2. Instruments

The transmission electron microscopy (TEM) images were collected on a Tecnai F20 transmission electron microscope (FEI, Hillsboro, OR, USA) operated at 120 kV. The scanning electron microscopy (SEM) images were collected on a SU8010 scanning electron microscope (Hitachi, Tokyo, Japan) operated at 2.0 kV. Zeta potential was carried out on a Malvern Zetasizer Nano ZS90 (UK). Atomic force microscopy (AFM) images were observed on a Bruker Multimode 8 AFM/SPM (Ettlingen, Germany) system in tapping mode and processed with freely available software: Gwyddion 2.30. The fluorescence spectra were measured using a SpectraMax M5 multi-mode microplate reader (Molecular Devices, San Jose, CA, USA) with the emission spectra ranging from 495 nm to 700 nm with an excitation of 485 nm at room temperature. The ultraviolet-visible (UV-Vis) absorption spectra were acquired from a DR6000 UV-Vis spectrophotometer (Hach, Loveland, CO, USA). Circular dichroism (CD) spectra were performed on a MOS-500 circular dichroism spectrometer (Bio-Logic, Seyssinet-Pariset, France) with a 0.1 cm quartz cell at 200—350 nm using standard procedures.

2.3. Synthesis of Cobalt Oxyhydroxide (CoOOH) Nanosheets

The CoOOH nanosheets were synthesized per a previously reported method [37]. First, 125 μL of sodium hydroxide (NaOH, 1 M) was added to 500 μL of $CoCl_2 \cdot 6H_2O$ solution (10 mM), and then the mixture was sonicated for 1 min. Then, 25 μL of sodium hypochlorite solution (NaClO, 0.9 M) was added to the mixture and sonicated for 10 min. Subsequently, the mixture was centrifuged at 14,000 rpm for 15 min and washed three times with deionized water. Finally, the product was re-dispersed in 1 mL of water to a final concentration of 0.25 mg/mL and stored at room temperature for further use.

2.4. Construction and Demonstration of Molecular Game-Theoretical System and Application in Sensing Metal Ions

Firstly, the T33 solution was diluted 100 μM to 100 nM using the Tris-HCl buffer solution (5 mM, pH 7.4). Then, 7.5 μL of CoOOH (0.25 mg/mL), after ultrasonication for 30 min, was added to 400 μL of T33 solution (100 nM), resulting in a T33–CoOOH complex (100 nM T33, 4.69 μg/mL CoOOH). The initial fluorescence spectrum of the T33–CoOOH mixture after 4 min of reaction was measured. Afterward, upon addition of different concentration of metal ions, the fluorescence spectra of T33 and the resulting T33–CoOOH complex were measured after 3 min of reaction. Finally, the fluorescence intensity was normalized and quenching ratio $(F0 - F)/F0$ was calculated.

2.5. Real Sample Analysis

A pond water sample from the Yuewang Pavilion of Hunan Normal University (Changsha, China) was filtered through a 0.2-μm membrane and then boiled for 5 min. Then, the pond water (5 μL) and standard solutions (5 μL) containing different amounts of Hg^{2+} were added into the T33–CoOOH complex (400 μL, 100 nM T33, 4.69 μg/mL CoOOH). After incubation for 3 min at room temperature, the fluorescence of the resulting mixtures was measured and calculated.

3. Results and Discussion

3.1. Construction and Characterization of Molecular Game-Theoretical System Based on Molecular Interactions

We first constructed an artificial molecular system based on molecular interactions among polythymine oligonucleotide T33, metal ions (Hg^{2+}), and CoOOH nanosheets (Figure 1). FAM-labeled T33 random coils in aqueous solution had strong fluorescence (normalized F = 1.0 a.u.) at 520 nm. Due to its unique fluorescence quenching and molecular adsorption capacities (Figure S1) [37], when positively charged hexagonal CoOOH nanosheets (TEM and SEM images in Figure S2A) were added into the solution, the negatively charged T33 adsorbed onto the surface of CoOOH nanosheets, resulting in fluorescence quenching (normalized F = 0.67 a.u., Figure 1a). This result may be attributed to the electrostatic adsorption (Figure S3) of T33 on CoOOH nanosheets and the effective fluorescence resonance energy transfer (FRET) between FAM and CoOOH nanosheets (Figure S2B) [38,39]. Only in the presence of Hg^{2+} did T33 change its conformation from a random coil to a T–Hg^{2+}–T hairpin structure, resulting in slight fluorescence quenching (normalized F = 0.96 a.u., Figure 1b). In the simultaneous presence of CoOOH and Hg^{2+}, Hg^{2+} may combine with T33 on the CoOOH nanosheets to form a T–Hg^{2+}–T hairpin structure, which increases the tightness of the bond of the three components, resulting in stronger quenching (normalized F = 0.3 a.u., Figure 1c).

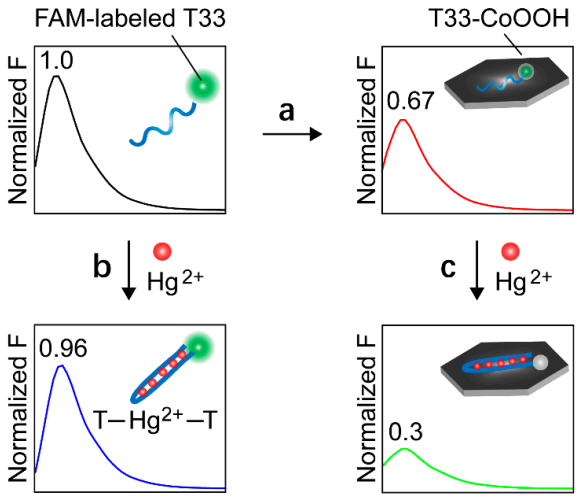

Figure 1. Schematic illustration and fluorescence emission spectra change of an artificial molecular system based on molecular interactions among polythymine oligonucleotide T33, metal ions (Hg^{2+}), CoOOH nanosheets. (**a**–**c**) the formation of T33–CoOOH (**a**); T–Hg^{2+}–T pairs (**b**); T33–CoOOH–Hg^{2+} (**c**). T33: 100 nM, CoOOH nanosheets: 4.69 μg/mL, Hg^{2+}: 10 μM. The excitation and emission wavelength are 485 and 520 nm. The fluorescence intensity is normalized. Buffer: 5 mM Tris-HCl buffer solution (pH 7.4); FAM: carboxyfluorescein; CoOOH: cobalt oxyhydroxide.

Atomic force microscopy (AFM), UV-Vis absorption spectroscopy, and CD) spectroscopy were used to characterize the above-mentioned molecular interaction process. The AFM results showed that the thickness of the CoOOH nanosheets was 12–16 nm (Figure 2A, n = 15). The thickness of the T33–CoOOH composites increased to 15–19 nm (Figure 2B, n = 15), indicating that T33 was adsorbed on the CoOOH nanosheets. The thickness of the T33–CoOOH–Hg^{2+} mixture increased to 21–23 nm (Figure 2C, n = 15). Figure 3A shows the absorption spectra of T33 and T33–CoOOH in the presence of various concentrations of Hg^{2+}. The optical density decreased as Hg^{2+} concentration increased and their absorption spectra displayed a slight redshift (264→270 nm, Figure 3A). In Figure 3B, CD spectra of T33 and T33–CoOOH in the presence of various concentrations of Hg^{2+} are shown. After the addition of Hg^{2+}, the positive band at 278 nm reduced. The experimental results clearly indicate the formation of T–Hg^{2+}–T pairs [40]. By further comparison with the fluorescence changes of free fluorescein, T3, and T33–CoOOH complex, at the different concentrations of Hg^{2+}, the fluorescence

of free fluorescein and T33 slightly decreased with increasing concentration of Hg^{2+} (Figure S4), indicating that the CoOOH nanosheets play an important role in enhancing the sensitivity of Hg^{2+} detection. We further investigated fluorescence responses of the T33–CoOOH complex to T33's fully complementary DNA A33. As a result, the formation of a T33–A33 duplex DNA also lead to similar quenching (normalized F from 0.67 to 0.51 a.u., Figure 3C). Thymine residues in T33 preferentially bind to Hg^{2+} through covalent N–Hg bonds [40]. Co^{3+} ions, which easily coordinate with nitrogen and oxygen atoms [41,42], likely bind to the remaining oxygen atoms of thymine residues. Thus, Hg^{2+} may combine with T33 on the CoOOH nanosheets to form a T–Hg^{2+}–T hairpin structure, which causes the three components to bind more tightly [43], probably due to the coordination of Co^{3+} of the CoOOH nanosheets to the oxygen atoms of T–Hg^{2+}–T complexes.

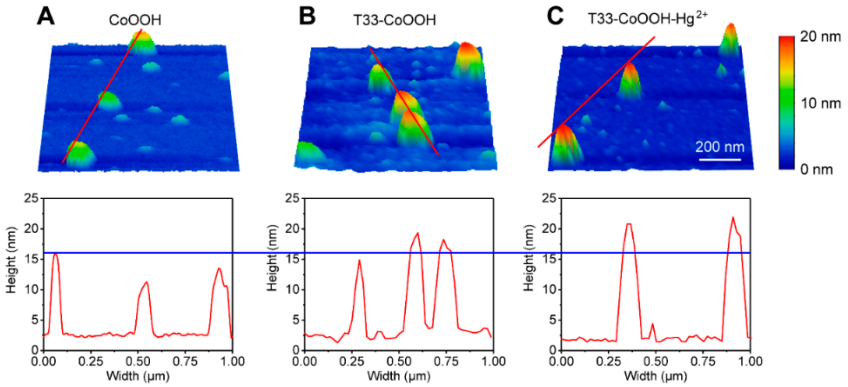

Figure 2. Representative atomic force microscopy (AFM) images and height analysis of (**A**) CoOOH; (**B**) T33–CoOOH; and (**C**) T33–CoOOH–Hg^{2+}.

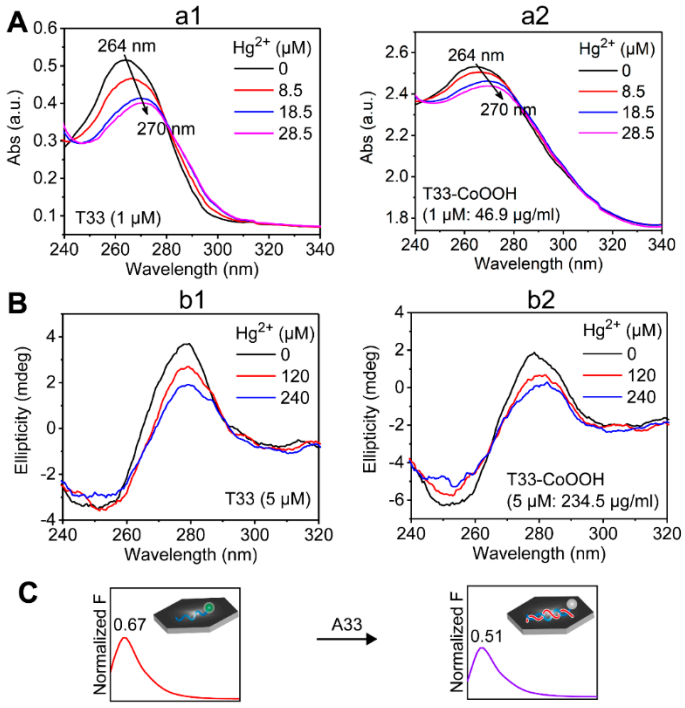

Figure 3. (**A**) Absorption response of T33 (a1, 1 μM) and T33–CoOOH (a2, 1 μM:46.9 μg/mL) on addition of Hg^{2+} ions; (**B**) CD spectra of T33 (b1, 5 μM) and T33–CoOOH (b2, 5 μM:234.5 μg/mL) on addition of Hg^{2+} ions. Buffer: 5 mM Tris-HCl, pH 7.4; (**C**) Fluorescence responses of the T33–CoOOH complex to T33's fully complementary DNA A33. T33: 100 nM, CoOOH nanosheets: 4.69 μg/mL, A33: 300 nM.

3.2. Demonstration of Molecular Game-Theoretical System

Game theory is an effective and powerful tool for analyzing strategic interactions between two or more agents or players. The prisoner's dilemma, a game theory classic, is a paradox in decision analysis in which acting for individual interests is pitted against acting for collective advantage. Generally, each player in the game chooses either "silence" or "betrayal" [21]. If both players are silent, they both receive the reward R. If both players betray, they both receive the punishment payoff P. If one betrays and the other keeps silent, the defector receives the temptation payoff T, while the silencer receives the "sucker's" payoff S. The rank order of payoffs (Figure 4A) is usually T > R > P > S. Because pursuing individual reward logically leads both players to betray, they would receive a better reward if both remain silent as 2R > T + S.

With the development of game theory in biology (especially at the cellular level), there are some predictions that game theory could be useful in the interpretation of molecular systems [1,6]. To extend game-theoretic treatment to an abiotic situation, our above-mentioned constructed artificial molecular system is a successful example of the application of game theory (prisoner's dilemma) to interactions among simple molecules, which relies on the hairpin structure of T33, specifically induced by Hg^{2+} and fluorescence quenching, and the molecular adsorption capacities of CoOOH nanosheets [37], resulting in fluorescence intensity and a distribution change in T33 (Figure 4B). From a game theory perspective, the molecular interaction of the "bait" molecule T33 with CoOOH and Hg^{2+} can be considered a "game" in which CoOOH and Hg^{2+} have two possible states: absence (silence) or presence (betrayal) regarded as two possible strategies, resulting in conflicts (sharing or self-interest) of the fluorescence distribution of T33, which conforms to the prisoner's dilemma. If both were absent (silent) and the bait molecule T33 did not interact with them, exhibiting its full fluorescence in which that payoff of the whole system was represented as 1, and then each molecular player was equivalent to share the average payoff R = 0.5. If one was absent (silent) and the other was present (betrayal), the existing one selfishly interacted with T33 to form the complex, resulting in fluorescence quenching. That is, in the presence (betrayal) of CoOOH and absence (silence) of Hg^{2+}, CoOOH selfishly owned the whole system's payoff T + S = 0.67 (note that T = 0.67, S = 0). Payoff S of Hg^{2+} was zero. Similarly, in the presence betrayal") of Hg^{2+} and absence (silence) of CoOOH, Hg^{2+} selfishly owned the whole system's payoff T + S = 0.96 (note that T = 0.96, S = 0), payoff S of CoOOH was zero. If both were present (betrayal), both competitively interacted with T33 to form T–Hg^{2+}–T–CoOOH ternary complex, resulting in stronger quenching of T33. Each molecular player received punishment (payoff P = 0.15), the payoff of the whole system was lowest (2P = 0.3). In this molecular game-theoretical system, the payoff of each molecular player is determined not only by its own state, but also by the state adopted by the molecular coplayers.

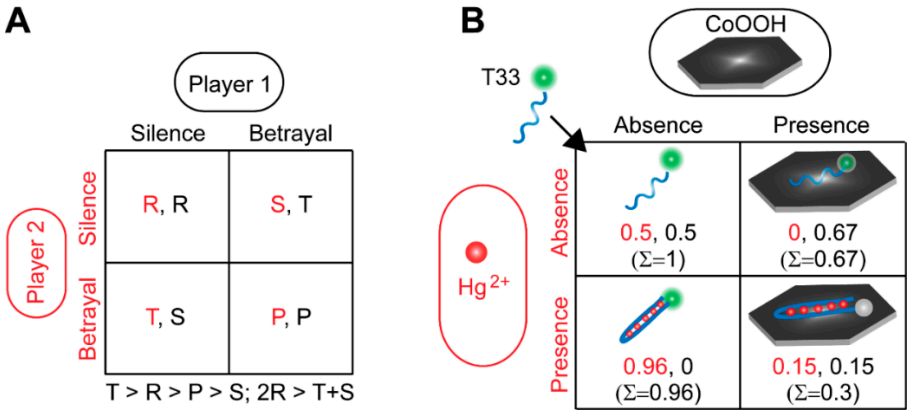

Figure 4. (**A**) Generalized payoff matrix for prisoner's dilemma where the two players are represented by red and black, and each player chooses to either silence or betrayal; (**B**) Realized payoff matrix for the molecular interaction of the bait molecule T33 with two molecular players, CoOOH and Hg^{2+}, with different states (absence = silence and presence = betrayal) regarded as strategies, resulting in conflicts (sharing or self-interest) of fluorescence distribution change of T33, which conforms to the prisoner's dilemma.

3.3. Molecular Game-Theoretical System for Sensing Hg^{2+}

According to the demonstration process of above-mentioned molecular game-theoretical system, both CoOOH and Hg^{2+} competitively interacted with T33 to form the T–Hg^{2+}–T–CoOOH ternary complex, resulting in the largest signal change (payoff from 2R = 1.0 to 2P = 0.3) of the whole system, suggesting that the T33–CoOOH complex sensitively senses Hg^{2+}. Under optimum conditions (100 nM T33, 4.69 μg/mL CoOOH, 5 mM Tris-HCl, pH 7.4, Figures S5 and S6), the T33–CoOOH complex was used for detection of Hg^{2+}. As shown in Figure 5A, the fluorescence intensity gradually decreased with increasing concentration of Hg^{2+} from 0 to 2000 nM. Similarly, the fluorescence quenching ratio (F0 − F)/F0 gradually increased with increasing concentration of Hg^{2+} from 0 to 2000 nM (Figure 5B). Figure 5C shows the good linear relationship between the value of (F0 − F)/F0 and the Hg^{2+} concentration in the range of 20 to 600 nM. The calibration equation was y = 0.00036x + 0.04076 with a correlation coefficient (R^2) of 0.995. The limit of detection was 7.94 nM according to the 3σ rule, which is below the maximum level (10 nM) of Hg^{2+} permitted by the U.S. Environmental Protection Agency for drinking water. Compared with other previously reported Hg^{2+} assays, our proposed approach has a much lower detection limit (Table S1). The result indicates that the molecular game-theoretical system based on T33 and CoOOH nanosheets can sensitively detect Hg^{2+}.

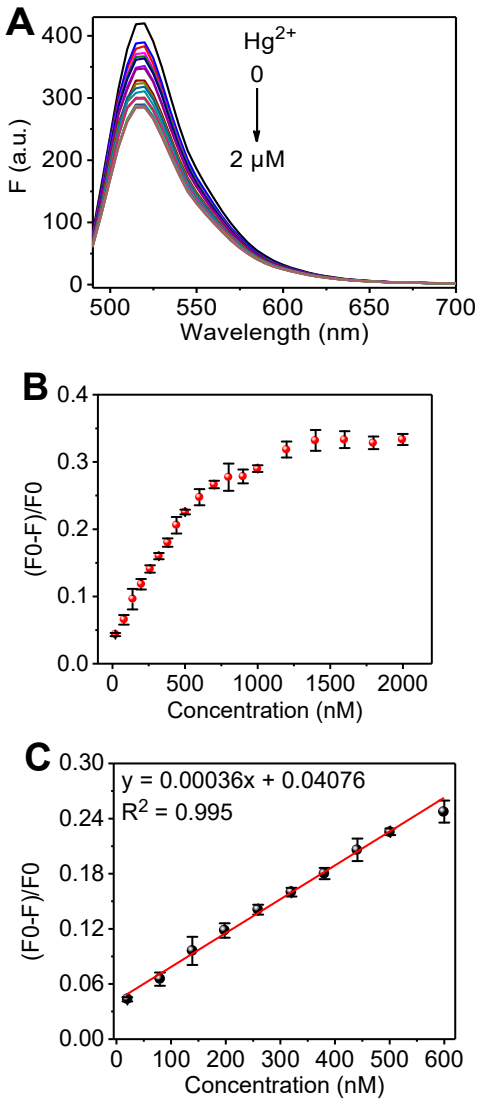

Figure 5. *Cont.*

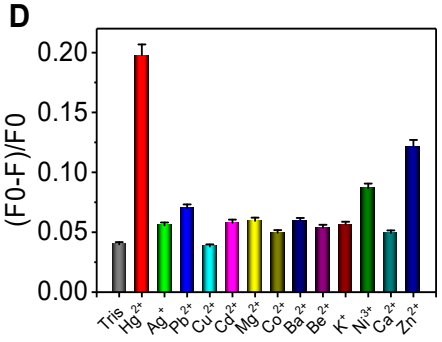

Figure 5. (**A**) Fluorescence emission spectra of T33–CoOOH complex (100 nM:4.69 μg/mL) upon addition of various concentrations of Hg^{2+} (from top to bottom: 0, 20, 80, 139, 198, 259, 320, 381, 441, 500, 600, 700, 800, 900, 1000, 1200, 1400, 1600, 1800, and 2000 nM); (**B**) The dependence of the fluorescence intensity changes (F0 − F)/F0 at 520 nm on the concentration of Hg^{2+}; (**C**) The linear relationship between (F0 − F)/F0 and the Hg^{2+} concentrations in the range from 20 to 600 nM; (**D**) The selectivity of the T33–CoOOH complex (100 nM:4.69 μg/mL) for Hg^{2+} assay (Hg^{2+}: 600 nM, other metal ions: 1.2 μM). Buffer: 5 mM Tris-HCl, pH 7.4.

To further evaluate the specificity of the T33–CoOOH complex under optimum conditions, we first investigated the responses of our method to Hg^{2+} (600 nM) against other metal ions (Ag^{+}, Pb^{2+}, Cu^{2+}, Cd^{2+}, Mg^{2+}, Co^{2+}, Ba^{2+}, Be^{2+}, K^{+}, Ni^{3+}, and Ca^{2+}; each 1.2 μM). As shown in the Figure 5D, the T33–CoOOH complex was highly selective for sensing Hg^{2+}, although the concentration of other interfering metal ions was much higher (two-fold) than that of Hg^{2+}. Zn^{2+} exhibited a certain degree of interference. Zn^{2+} may incorporate into CoOOH for formation of Zn-doped CoOOH [44,45] and Zn-doped CoOOH may bind to thymines, probably by interacting with the Zn^{2+} metal center with the deprotonated N3 imide of thymine and stacking the aromatic pendent group on the thymine nucleobase [46,47].

A competition experiment in the presence of potentially competitive metal ions was also performed to further confirm the selectivity of this sensing system toward Hg^{2+}. As shown in Figure S7A, Hg^{2+} can efficiently quench the fluorescence of this sensing system even if the other metal ions slightly affected the fluorescence intensity. As shown in Figure S7B, common anions did not remarkably affect the fluorescence change. In addition, the fluorescence quenching ratio (F0 − F)/F0 gradually increased with increasing concentration of A33 from 20 to 270 nM, and there was a good linear relationship between the quenching ratio (F0 − F)/F0 and the A33 concentration in the range of 20 to 270 nM (y = 0.00091x + 0.00447, R^2 = 0.992, Figure S8).

We applied the T33–CoOOH complex to determinate the concentration of Hg^{2+} in pond water, to evaluate its performance in a real water sample. In order to avoid the adverse effects of sediments and nucleases in the real water sample on the sensing system, we first filtered and boiled the real water sample. As shown in Table 1, the spike recovery for Hg^{2+} in the concentration ranged from 104.93 to 108.29%, and the relative standard deviation (RSD) ranged from 0.59 to 1.15%, which indicated the developed method has great potential for detection Hg^{2+} in real water samples.

Table 1. Determination of Hg^{2+} in real water samples (n = 3).

Sample	Added (nM)	Found (nM)	Recovery (%)	RSD (%)
Pond water	84.00	90.96	108.29	0.59
	155.00	162.64	104.93	1.15

4. Conclusions

In summary, we demonstrated a proof-of-concept molecular game-theoretical system (molecular prisoner's dilemma) that relies on the formation of the T–Hg^{2+}–T hairpin structure specifically induced

by Hg^{2+} and fluorescence quenching and molecular adsorption capacities of CoOOH nanosheets, resulting in fluorescence intensity and distribution change in polythymine oligonucleotide T33. The bait molecule T33 interacted with two molecular players, CoOOH and Hg^{2+}, with different states (absence = silence and presence = betrayal) regarded as strategies, and created conflicts (sharing or self-interest) of fluorescence distribution of T33, quantifiable in a 2 × 2 payoff matrix. The molecular game-theoretical system based on T33 and CoOOH was used for sensing Hg^{2+} in the range of 20 to 600 nM with a detection limit of 7.94 nM (3σ) and for determination of Hg^{2+} in pond water. Although the demonstrated molecular game system is relatively simple, it has high versatility and broad applicability and can be extended to various other molecular systems, such as RNA/DNA/peptide-based systems, nano-based systems, host–guest supramolecular systems, and solid-phase molecular self-assembly systems. Inspired by the proof-of-concept for the feasibility of molecular game theory, a variety of molecular decision-making platforms will be developed, which will help promote molecular information processing and generating novel molecular intelligent decision systems for environmental monitoring and molecular diagnosis and therapy.

Supplementary Materials: The following are available online at http://www.mdpi.com/2076-3417/8/12/2530/s1, Figure S1: Comparison of fluorescence quenching ability of CoOOH to different fluorescence dyes. Figure S2: Characterization of CoOOH nanosheets. Figure S3: Comparison of ζ-potential for CoOOH, T33–CoOOH, and T33–CoOOH–Hg^{2+} mixtures. Figure S4: Comparison of fluorescence changes in free fluorescein, T33, and T33–CoOOH complexes at different concentrations of Hg^{2+}. Figure S5: Optimization of the concentration of CoOOH nanosheets. Figure S6: Optimization of reaction time. Figure S7: Competition experiment and the interference of anions. Figure S8: T33–CoOOH complexes for detection of A33 DNA. Table S1: Comparison of the detection slimit and linear ranges of other reported Hg^{2+} assays.

Author Contributions: W.T.H. designed the methods, N.F.N. and X.X.Z. performed the experiments, and optimized the parameters; C.S.F., Q.Y.Z., J.Y.L., F.R.Z., and Q.F.Y. optimized the process and analyzed the data, W.T.H. and N.F.N wrote the paper; X.Z.D. and L.Q.X. performed review and editing. The first two authors contributed equally to this paper.

Funding: This work was supported by the National Natural Science Foundation of China (No. 21505042), Scientific and Technological Plan Project of Changsha of China (No. KQ1707010 and KQ1802046), Hunan Provincial Natural Science Foundation of China (No. 2016JJ3084), the Research Foundation of Education Bureau of Hunan Province (No. 15K084), the Cooperative Innovation Center of Engineering and New Products for Developmental Biology of Hunan Province (No. 20134486), and College Student Innovative Experiment Project of Hunan Province (No. 2017106).

Conflicts of Interest: The authors declare no conflict of interest.

References

1. Hummert, S.; Bohl, K.; Basanta, D.; Deutsch, A.; Werner, S.; Theissen, G.; Schroeter, A.; Schuster, S. Evolutionary game theory: Cells as players. *Mol. Biosyst.* **2014**, *10*, 3044–3065. [CrossRef]
2. Sanfey, A.G. Social Decision-Making: Insights from Game Theory and Neuroscience. *Science* **2007**, *318*, 598–602. [CrossRef]
3. Nowak, M.A.; Sasaki, A.; Taylor, C.; Fudenberg, D. Emergence of cooperation and evolutionary stability in finite populations. *Nature* **2004**, *428*, 646–650. [CrossRef]
4. Yeates, J.A.M.; Hilbe, C.; Zwick, M.; Nowak, M.A.; Lehman, N. Dynamics of prebiotic RNA reproduction illuminated by chemical game theory. *Proc. Natl. Acad. Sci. USA* **2016**, *113*, 5030–5035. [CrossRef]
5. Turner, P.E.; Chao, L. Prisoner's dilemma in an RNA virus. *Nature* **1999**, *398*, 441–443. [CrossRef]
6. Bohl, K.; Hummert, S.; Werner, S.; Basanta, D.; Deutsch, A.; Schuster, S.; Theissen, G.; Schroeter, A. Evolutionary game theory: Molecules as players. *Mol. Biosyst.* **2014**, *10*, 3066–3074. [CrossRef]
7. Vaidya, N.; Manapat, M.L.; Chen, I.A.; Xulvi-Brunet, R.; Hayden, E.J.; Lehman, N. Spontaneous network formation among cooperative RNA replicators. *Nature* **2012**, *491*, 72–77. [CrossRef]
8. Feynman, R.P. There's plenty of room at the bottom: An invitation to enter a new field of physics. In *Handbook of Nanoscience, Engineering, and Technology*, 3rd ed.; CRC Press: Boca Raton, FL, USA, 2012; pp. 26–35.
9. Nurse, P. Life, logic and information. *Nature* **2008**, *454*, 424–426. [CrossRef]
10. Ausländer, D.; Ausländer, S.; Pierrat, X.; Hellmann, L.; Rachid, L.; Fussenegger, M. Programmable full-adder computations in communicating three-dimensional cell cultures. *Nat. Methods* **2017**, *15*, 57–60. [CrossRef]

11. Green, A.A.; Kim, J.; Ma, D.; Silver, P.A.; Collins, J.J.; Yin, P. Complex cellular logic computation using ribocomputing devices. *Nature* **2017**, *548*, 117–121. [CrossRef]
12. Erbas-Cakmak, S.; Kolemen, S.; Sedgwick, A.C.; Gunnlaugsson, T.; James, T.D.; Yoon, J.; Akkaya, E.U. Molecular logic gates: The past, present and future. *Chem. Soc. Rev.* **2018**, *47*, 2228–2248. [CrossRef]
13. Szaciłowski, K. Digital Information Processing in Molecular Systems. *Chem. Rev.* **2008**, *108*, 3481–3548. [CrossRef]
14. Cherry, K.M.; Qian, L. Scaling up molecular pattern recognition with DNA-based winner-take-all neural networks. *Nature* **2018**, *559*, 370–376. [CrossRef]
15. Qian, L.; Winfree, E.; Bruck, J. Neural network computation with DNA strand displacement cascades. *Nature* **2011**, *475*, 368–372. [CrossRef]
16. Boukis, A.C.; Reiter, K.; Froelich, M.; Hofheinz, D.; Meier, M.A.R. Multicomponent reactions provide key molecules for secret communication. *Nat. Commun.* **2018**, *9*, 1439. [CrossRef]
17. Lustgarten, O.; Motiei, L.; Margulies, D. User Authorization at the Molecular Scale. *ChemPhysChem* **2017**, *18*, 1678–1687. [CrossRef]
18. Huang, W.T.; Chen, L.X.; Lei, J.L.; Luo, H.Q.; Li, N.B. Molecular neuron: From sensing to logic computation, information encoding, and encryption. *Sens. Actuator B-Chem.* **2017**, *239*, 704–710. [CrossRef]
19. Andréasson, J.; Pischel, U. Molecules for security measures: From keypad locks to advanced communication protocols. *Chem. Soc. Rev.* **2018**, *47*, 2266–2279. [CrossRef]
20. Chatterjee, G.; Dalchau, N.; Muscat, R.A.; Phillips, A.; Seelig, G. A spatially localized architecture for fast and modular DNA computing. *Nat. Nanotechnol.* **2017**, *12*, 920–927. [CrossRef]
21. Schuster, S.; Kreft, J.U.; Schroeter, A.; Pfeiffer, T. Use of Game-Theoretical Methods in Biochemistry and Biophysics. *J. Biol. Phys.* **2008**, *34*, 1–17. [CrossRef]
22. Liu, J.; Cao, Z.; Lu, Y. Functional Nucleic Acid Sensors. *Chem. Rev.* **2009**, *109*, 1948–1998. [CrossRef] [PubMed]
23. Zhang, X.B.; Kong, R.M.; Lu, Y. Metal Ion Sensors Based on DNAzymes and Related DNA Molecules. *Ann. Rev. Anal. Chem.* **2011**, *4*, 105–128. [CrossRef] [PubMed]
24. Li, L.; Wen, Y.; Xu, L.; Xu, Q.; Song, S.; Zuo, X.; Yan, J.; Zhang, W.; Liu, G. Development of mercury (II) ion biosensors based on mercury-specific oligonucleotide probes. *Biosens. Bioelectron.* **2016**, *75*, 433–445. [CrossRef] [PubMed]
25. Park, K.S.; Jung, C.; Park, H.G. "Illusionary" Polymerase Activity Triggered by Metal Ions: Use for Molecular Logic-Gate Operations. *Angew. Chem. Int. Ed.* **2010**, *49*, 9757–9760. [CrossRef] [PubMed]
26. Liu, J.; Lu, Y. Rational Design of "Turn-On" Allosteric DNAzyme Catalytic Beacons for Aqueous Mercury Ions with Ultrahigh Sensitivity and Selectivity. *Angew. Chem. Int. Ed.* **2007**, *46*, 7587–7590. [CrossRef] [PubMed]
27. Li, J.; Lu, L.; Kang, T.; Cheng, S. Intense charge transfer surface based on graphene and thymine–Hg(II)–thymine base pairs for detection of Hg^{2+}. *Biosens. Bioelectron.* **2016**, *77*, 740–745. [CrossRef] [PubMed]
28. Zhu, Z.; Su, Y.; Li, J.; Li, D.; Zhang, J.; Song, S.; Zhao, Y.; Li, G.; Fan, C. Highly Sensitive Electrochemical Sensor for Mercury(II) Ions by Using a Mercury-Specific Oligonucleotide Probe and Gold Nanoparticle-Based Amplification. *Anal. Chem.* **2009**, *81*, 7660–7666. [CrossRef]
29. Chiang, C.K.; Huang, C.C.; Liu, C.W.; Chang, H.T. Oligonucleotide-based fluorescence probe for sensitive and selective detection of mercury (II) in aqueous solution. *Anal. Chem.* **2008**, *80*, 3716–3721. [CrossRef]
30. Chen, G.H.; Chen, W.Y.; Yen, Y.C.; Wang, C.W.; Chang, H.T.; Chen, C.F. Detection of mercury (II) ions using colorimetric gold nanoparticles on paper-based analytical devices. *Anal. Chem.* **2014**, *86*, 6843–6849. [CrossRef]
31. Xie, W.Y.; Huang, W.T.; Zhang, J.R.; Luo, H.Q.; Li, N.B. A triple-channel optical signal probe for Hg^{2+} detection based on acridine orange and aptamer-wrapped gold nanoparticles. *J. Mater. Chem.* **2012**, *22*, 11479–11482. [CrossRef]
32. Zhang, J.R.; Huang, W.T.; Xie, W.Y.; Wen, T.; Luo, H.Q.; Li, N.B. Highly sensitive, selective, and rapid fluorescence Hg^{2+} sensor based on DNA duplexes of poly(dT) and graphene oxide. *Analyst* **2012**, *137*, 3300–3305. [CrossRef] [PubMed]
33. Srinivasan, K.; Subramanian, K.; Murugan, K.; Dinakaran, K. Sensitive fluorescence detection of mercury(ii) in aqueous solution by the fluorescence quenching effect of MoS2 with DNA functionalized carbon dots. *Analyst* **2016**, *141*, 6344–6352. [CrossRef] [PubMed]

34. Xie, W.Y.; Huang, W.T.; Luo, H.Q.; Li, N.B. CTAB-capped Mn-doped ZnS quantum dots and label-free aptamer for room-temperature phosphorescence detection of mercury ions. *Analyst* **2012**, *137*, 4651–4653. [CrossRef] [PubMed]
35. Zhang, J.R.; Huang, W.T.; Zeng, A.L.; Luo, H.Q.; Li, N.B. Ethynyl and pi-stacked thymine-Hg^{2+}-thymine base pairs enhanced fluorescence quenching via photoinduced electron transfer and simple and sensitive mercury ion sensing. *Biosens. Bioelectron.* **2015**, *64*, 597–604. [CrossRef] [PubMed]
36. Shankar, B.H.; Jayaram, D.T.; Ramaiah, D. A Reversible Dual Mode Chemodosimeter for the Detection of Cyanide Ions in Natural Sources. *Chem. Asian J.* **2014**, *9*, 1636–1642. [CrossRef] [PubMed]
37. Li, N.; Li, Y.H.; Han, Y.Y.; Pan, W.; Zhang, T.T.; Tang, B. A Highly Selective and Instantaneous Nanoprobe for Detection and Imaging of Ascorbic Acid in Living Cells and in Vivo. *Anal. Chem.* **2014**, *86*, 3924–3930. [CrossRef] [PubMed]
38. Cen, Y.; Yang, Y.; Yu, R.Q.; Chen, T.T.; Chu, X. A cobalt oxyhydroxide nanoflake-based nanoprobe for the sensitive fluorescence detection of T4 polynucleotide kinase activity and inhibition. *Nanoscale* **2016**, *8*, 8202–8209. [CrossRef] [PubMed]
39. Chang, Y.Q.; Zhang, Z.; Liu, H.Q.; Wang, N.; Tang, J.L. Cobalt oxyhydroxide nanoflake based fluorescence sensing platform for label-free detection of DNA. *Analyst* **2016**, *141*, 4719–4724. [CrossRef]
40. Miyake, Y.; Togashi, H.; Tashiro, M.; Yamaguchi, H.; Oda, S.; Kudo, M.; Tanaka, Y.; Kondo, Y.; Sawa, R.; Fujimoto, T.; et al. MercuryII-Mediated Formation of Thymine−HgII−Thymine Base Pairs in DNA Duplexes. *J. Am. Chem. Soc.* **2006**, *128*, 2172–2173. [CrossRef]
41. Chang, E.L.; Simmers, C.; Knight, D.A. Cobalt Complexes as Antiviral and Antibacterial Agents. *Pharmaceuticals (Basel)* **2010**, *3*, 1711–1728. [CrossRef]
42. Francisco, T.M.; Gee, W.J.; Shepherd, H.J.; Warren, M.R.; Shultz, D.A.; Raithby, P.R.; Pinheiro, C.B. Hard X-ray-Induced Valence Tautomeric Interconversion in Cobalt-o-Dioxolene Complexes. *J. Phys. Chem. Lett.* **2017**, *8*, 4774–4778. [CrossRef] [PubMed]
43. Zhang, X.X.; Zhu, Q.Y.; Lu, J.Y.; Zhang, F.R.; Huang, W.T.; Ding, X.Z.; Xia, L.Q. Boolean logic tree of molecular self-assembly system based on cobalt oxyhydroxide nanoflakes for three-state logic computation, sensing and imaging of pyrophosphate in living cells and in vivo. *Analyst* **2018**. [CrossRef] [PubMed]
44. Wang, J.S.; Liu, J.; Zhang, B.; Cheng, F.; Ruan, Y.J.; Ji, X.; Xu, K.; Chen, C.; Miao, L.; Jiang, J.J. Stabilizing the oxygen vacancies and promoting water-oxidation kinetics in cobalt oxides by lower valence-state doping. *Nano Energy* **2018**, *53*, 144–151. [CrossRef]
45. Wang, J.W.; Kuo, Y.M. Synthesis of Nanosized Zinc-Doped Cobalt Oxyhydroxide Parties by a Dropping Method and Their Carbon Monoxide Gas Sensing Properties. *J. Nanomater.* **2013**, 136145. [CrossRef]
46. Aoki, S.; Kimura, E. Zinc-nucleic acid interaction. *Chem. Rev.* **2004**, *104*, 769–787. [CrossRef] [PubMed]
47. Sander, S.A.; Van Hall, A.K.; Morrow, J.R. Zn^{2+}-Selective Switch of Duplex to Hairpin DNA. *Inorg. Chem.* **2015**, *54*, 3084–3086. [CrossRef] [PubMed]